Proposal to Jefferson Lab PAC 40

CREX: PARITY-VIOLATING MEASUREMENT of the WEAK CHARGE DISTRIBUTION of ^{48}Ca to 0.02 fm ACCURACY

Spokespersons: J. Mammei, D. McNulty, R. Michaels, K. Paschke, S. Riordan*, P.A. Souder

J. Mammei, J. Birchall, M. Gericke, R. Mahurin, W.T.H. van Oers, S. Page
University of Manitoba

S. Riordan, P. Decowski, K. Kumar, T. Kutz, J. Wexler
University of Massachusetts, Amherst

K. Paschke, G.D. Cates, M. Dalton, D. Keller, X. Zheng
University of Virginia

P.A. Souder, R. Beminiwattha, R. Holmes
Syracuse University

R. Michaels, K. Allada, J. Benesch, A. Camsonne, J.P. Chen, D. Gaskell,
J. Gomez, O. Hansen, D.W. Higinbotham, C.E. Keppel, J. LeRose, B. Moffit
S. Nanda, P. Solvignon-Slifer, B. Wojtsekhowski, J. Zhang
Thomas Jefferson National Accelerator Facility

Konrad Aniol
California State University, Los Angeles

G.B. Franklin, B. Quinn
Carnegie Mellon Univerisity

D. Watts, L. Zana
The University of Edinburgh

P. Markowitz
Florida International University

*contact spokesperson, riordan@jlab.org

P. Gueye
Hampton University

E. Cisbani, A. del Dotto, S. Frullani, F. Garibaldi
INFN Roma gruppo collegato Sanità
and Italian National Institute of Health, Rome, Italy

M. Capogni
INFN Roma gruppo collegato Sanità
and ENEA Casaccia, Rome, Italy

V. Bellini, A. Giusa, F. Mammoliti, G. Russo, M.L. Sperduto, C.M. Sutera
INFN - Sezione di Catania

D. McNulty, P. Cole, T. Forest, M. Khandaker
Idaho State University

C.J. Horowitz
Indiana University

M. Mihovilovič, S. Širca
Jožef Stefan Institute and University of Ljubljana, Slovenia

A. Glamazdin
Kharkov Institute of Physics and Technology

T. Holmstrom
Longwood University

S. Kowalski, R. Silwal, V. Sulkosky
Massachusetts Institute of Technology

M. Shabestari
Mississippi State University

S.K. Phillips
University of New Hampshire

E. Korkmaz
University of Nortern British Columbia

P. King, J. Roche, B. Waidyawansa
Ohio University

C.E. Hyde
Old Dominion University

F. Meddi, G.M. Urciuoli
Sapienza University of Rome and INFN - Sezione di Roma

A. Blomberg, Z.-E. Meziani, N. Sparveris
Temple University

M. Pitt
Viriginia Polytechnic Institute and State University

D. Armstrong, J.C. Cornejo, W. Deconinck, J.F. Dowd, V. Gray, and J. Magee
College of William and Mary

D. Androic
University of Zagreb

A Hall A Collaboration Proposal

We gratefully acknowledge J. Piekarewicz and W. Nazarewicz for important contributions to Section I and G. Hagen for providing preliminary coupled cluster calculation results. Finally, we thank Jefferson Lab for supporting the CREX workshop where this proposal was discussed.

The proposal and related information is at
http://hallaweb.jlab.org/parity/prex

ABSTRACT

The ^{48}Ca Radius EXperiment (CREX) was conditionally approved at the C2 level by PAC39, which recommended that a stronger case be made demonstrating "how the ^{48}Ca result will test microscopic models." In order to evaluate the case, a workshop was held at Jefferson Lab in March 2013 [1] with leading theorists from several fields that have an interest in our proposal. The status of these microscopic calculations was presented and the results of these calculations are expected to be available by the time the experiment will run. The conclusion of the workshop was that a measurement of the neutron skin of ^{48}Ca with a precision of 0.02 fm will be an essential benchmark in the field.

We propose to measure the parity-violating asymmetry for elastic scattering from ^{48}Ca at E = 2.2 GeV and $\theta = 4^{\circ}$. This will provide a measurement of the weak charge distribution and hence the neutron density at one value of Q^2 = 0.022 (GeV/c)^2. It will provide an accuracy in the ^{48}Ca neutron radius R_n^{48} equivalent to $\pm$0.02 fm ($\sim 0.6\%$). A measurement this precise will have a significant impact on nuclear theory, providing unique experimental input to help bridge ab-initio theoretical approaches (based on nucleon-nucleon and three-nucleon forces) and the nuclear density functional theory (based on energy density functionals). Together with the planned ^{208}Pb neutron radius measurement (R_n^{208}), R_n^{48} will provide unique input in such diverse areas such as neutron star structure, heavy ion collisions, and atomic parity violation. A precise measurement on a small nucleus is favorable because it can be measured at high momentum transfer where the asymmetry is larger (for the proposed kinematics, about 2 ppm). Also, since ^{48}Ca is neutron-rich it has a larger weak charge and greater sensitivity to R_n. We are requesting 45 days of polarized beam running in Hall A at a 1-pass energy of 2.2 GeV using a septum magnet to reach a 4° scattering angle. The experimental setup is similar to PREX. This beam time request includes 35 days of production data-taking and 5 days of commissioning and 5 days of overhead for Møller polarimetry and other auxiliary measurements.

1 Scientific Motivation

The proposed measurement to determine the parity-violating asymmetry in elastic scattering from ^{48}Ca nuclei with a total error of 2.4% at $q \sim 0.8$ fm^{-1}, from which a measurement of the neutron RMS radius R_n can be extracted with an accuracy of ± 0.02 fm, would make a unique contribution to one of the overarching goals of Jefferson Laboratory, namely to understand the structure of complex hadrons in terms of fundamental strong interaction physics.

One important aspect of achieving this goal is the bridging of different descriptions of hadronic systems that are applicable at different resolutions, Fig. 1. While Lattice QCD provides an accurate description of single nucleons and may provide information on two-nucleon (NN) and three-nucleon (3N) interactions, chiral effective field theory, coupled with improved ab initio many-body calculations, describes the structure of light to medium-mass nuclei in terms of NN and 3N forces [2]. The nuclear density functional theory (DFT) [3], while applicable to the whole nuclear landscape, works best in medium and heavy nuclei where the concept of a nuclear mean field is more appropriate [4, 5].

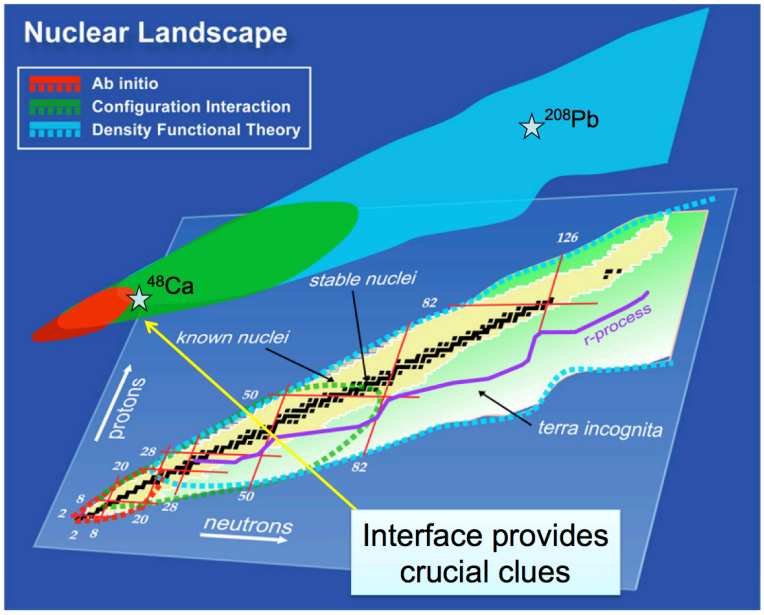

Figure 1: Nuclear landscape in a (Z, N) plane. Light nuclei are best described by ab initio methods based on inter-nucleon forces. Heavier nuclei are best described by nuclear DFT. The parity violating electron scattering experiments PREX on ^{208}Pb and CREX (this proposal) on ^{48}Ca are indicated by stars. The CREX data will help bridge ab initio and DFT approaches. (Based on Ref. [4].)

Together these theories accurately predict isoscalar properties of nuclei (where neutrons and protons contribute coherently) across the whole the nuclear landscape. For example, binding energies of stable nuclei are primarily isoscalar. However, presently we have limited numbers of accurate isovector observables (where neutrons and protons contribute with opposite sign) that can be used to test and constrain isovector parts of density functionals [6] or the poorly known isospin $T = 3/2$ component of the 3N force [7, 8].

The neutron skin $R_n - R_p$, the difference in RMS radii of the neutron and proton densities (R_n and R_p respectively), which can be extracted cleanly from the proposed measurement of the parity-violating asymme-

try, is an unique isovector observable of great importance for nuclear theory. Recently the PREX experiment pioneered this technique to extract R_n for ^{208}Pb. This doubly-magic heavy nucleus can be well-described by DFT, thus relating $R_n(^{208}\text{Pb})$ to bulk properties of neutron rich matter such as the density dependence of the symmetry energy. However, ^{208}Pb with 208 nucleons is presently beyond the capabilities of ab initio calculations, rendering a direct relationship to crucial $T = 3/2$ forces [7, 8] difficult.

To provide a key information for bridging DFT and ab initio approaches, we seek a stable, lighter, neutron-rich nucleus, with a simple doubly closed shell structure. This leaves us with only one choice: ^{48}Ca. With 48 nucleons, ^{48}Ca is light enough to provide this bridge, as illustrated in Fig. 1. Not only is the extraction of R_n from ^{48}Ca a theoretical meeting ground, but neutron-rich Ca isotopes are the focus of several recent experimental measurements with radioactive beams [9]. Indeed, the combination of parity-violating asymmetry measurements such as PREX and CREX on stable nuclei and measurements of observables involving very neutron rich unstable nuclei form a powerful complementary set of inputs to nuclear theory.

A precise measurement of the parity-violating asymmetry at an optimum value of Q^2 is feasible using a high current longitudinally polarized 2.2 GeV electron beam and the HRS spectrometer pair in Hall A. In the following, we first introduce the concept of the proposed measurement on ^{48}Ca and review the ongoing PREX measurement on ^{208}Pb. We then describe how CREX can build on the PREX measurement to provide tests of DFTs and microscopic calculations and thus provide valuable new insight into the structure of nuclei.

1.1 Partiy-Violating Asymmetries, Neutron Densities and the CREX Measurement

In the Born approximation, elastic electron scattering probes directly the charge form factor $F_{ch}(Q^2)$ of the nucleus. In turn, the charge density ρ_{ch} may be obtained by taking the Fourier transform of $F_{ch}(Q^2)$. Indeed, an extensive set of measurements covering a large range of Q^2 and many isotopes has provided a detailed picture of the sizes and shapes of nuclei [10]. Since the electron interacts with the nucleus through the well-known electromagnetic interaction, the interpretation of these results are theoretically clean. In contrast, our knowledge of neutron densities comes primarily from hadron scattering experiments involving, for example, pions [11], protons [12, 13, 14], antiprotons [15, 16] or alpha particles [17, 18], the interpretation of which requires a model-dependent description of the non-perturbative strong interaction.

An alternative approach is to exploit the fact that the Z-boson couples much more strongly to neutrons than protons ($Q_W^p \approx 1 - 4\sin^2\theta_W \ll |Q_W^n| \approx 1$, where $Q_W^{p,n}$ are the nucleon weak charges), so parity violation in elastic electron scattering is sensitive to the neutron density distribution ρ_n. Given the electroweak character of the interaction, the measurement of parity violation in electron scattering provides a model-independent probe of neutron densities that is free from most strong interaction uncertainties [19].

In the Born approximation, the parity-violating asymmetry of the cross section for longitudinally polarized electrons elastically scattered from an unpolarized nucleus, A_{PV}, is proportional to the weak form factor $F_W(Q^2)$, Fig. 2. This is the Fourier transform of the weak charge density, which is closely related to the neutron density because of the weakness of the proton weak charge. Thus, the neutron density can be extracted cleanly from an electroweak measurement [19].

In the limit $Q^2 \ll M_Z^2$, this asymmetry is given by

$$A_{PV} = \frac{\sigma_R - \sigma_L}{\sigma_R + \sigma_L} \approx \frac{G_F Q^2}{4\pi\alpha\sqrt{2}} \frac{F_W(Q^2)}{F_{ch}(Q^2)}, \tag{1}$$

where $\sigma_{R(L)}$ is the differential cross section for elastic scattering of right- (R) and left- (L) handed longitudi-

nally polarized electrons, G_F is the Fermi constant, α the fine structure constant, and $F_{ch}(Q^2)$ is the Fourier transform of the known charge density. We propose to make a measurement of A_{PV} with a total error of 2.4%, from which a measurement of F_W can be extracted at $q \sim 0.8$ fm^{-1}, yielding an R_n measurement with an total error of ± 0.02 fm.

For a heavy nucleus, Coulomb-distortion effects are large and must be included. These have been accurately calculated [20] exploiting the fact that the charge density is well known. Many other details relevant for a practical parity violation experiment to measure neutron densities have been discussed in a previous publication [21].

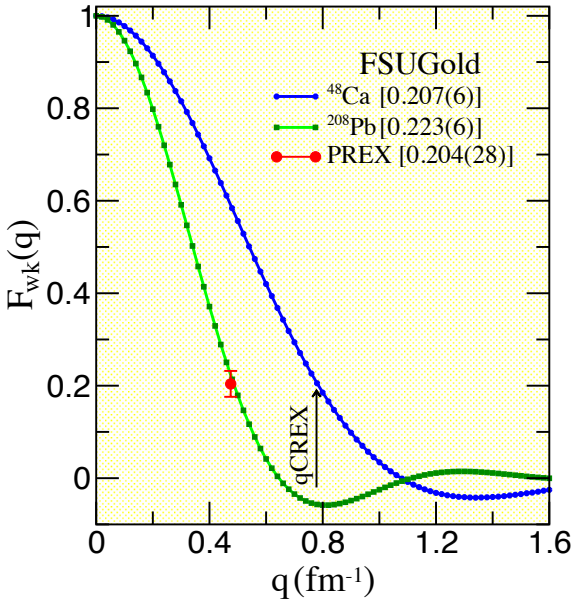

Figure 2: Weak form factors, the Fourier transform of weak charge density, for ^{208}Pb and ^{48}Ca vs. momentum transfer as predicted by the relativistic mean field interaction FSUGold [22, 23]. The PREX result (red error bar) and the proposed momentum transfer for CREX are also shown.

The weak radius is proportional to the derivative of F_W with respect to Q^2, evaluated at $Q^2 = 0$. While the proposed measurement will be carried out at a finite (but small) Q^2, leading in principle to some small uncertainty stemming from the unknown surface thickness of the weak charge distribution, direct theoretical model comparisons can be made with F_W itself. The essential point is that if a theoretical model can predict the weak radius, the model can almost certainly also predict the weak form factor. Both the radius and form factor are calculated by integrating over the theoretical density distribution. In Fig. 3 we show the very strong Pearson correlation coefficient [6] between the neutron radius and the weak form factor for both ^{48}Ca and ^{208}Pb as predicted by the relativistic mean field interaction FSUGold.

1.2 The PREX and PREX-II Experiments on ^{208}Pb

In this section we briefly review the motivation for and the results of the related experiments PREX and PREX-II. For neutron-rich nuclei, some of the excess neutrons are expected to be found in the surface, where they form a neutron-rich skin. The thickness of this skin, $R_n - R_p$, is primarily sensitive to isovector

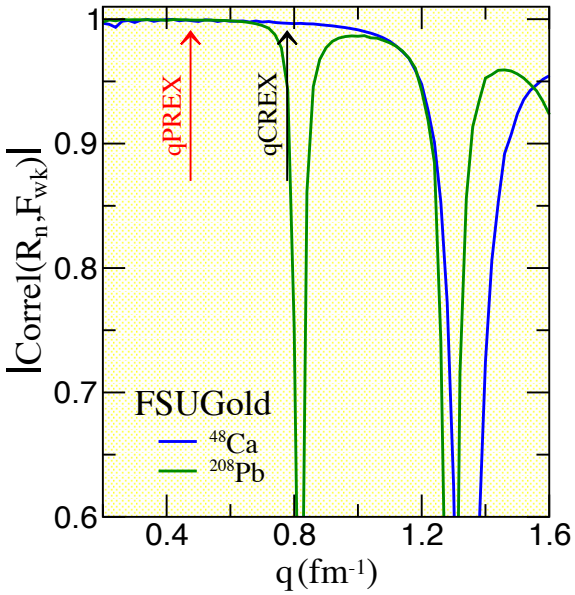

Figure 3: The correlation between the neutron radius R_n and the weak form factor as a function of momentum transfer predicted by the relativistic mean field interaction FSUGold for ^{48}Ca blue and ^{208}Pb green [23].

dynamics and provides fundamental nuclear structure information. This insight motivated the PREX and PREX-II experiments on ^{208}Pb. Note that there is a strong correlation between the neutron radius in ^{208}Pb, R_n^{208}, and the pressure of neutron matter P at densities near 0.1 fm^{-3} (about 2/3 of nuclear saturation density) [24]. A larger P will push neutrons out against surface tension and increase R_n. Therefore measuring R_n^{208} constrains the equation-of-state (EOS), the pressure as a function of density, of neutron matter. Given that the same pressure pushes neutrons against gravity in a neutron star, PREX and PREX-II place important constraints on neutron stars [25, 26, 27, 28, 29, 30]. Moreover, insights from these experiments constrain how efficiently isospin equilibrates in heavy-ion collisions [31, 32].

The PREX experiment measured the parity-violating asymmetry A_{PV} for 1.06 GeV electrons scattered by about five degrees from ^{208}Pb, with the result [33]

$$A_{PV} = 0.656 \pm 0.060(\text{stat}) \pm 0.014(\text{syst}) \text{ ppm}\,. \tag{2}$$

A major success of PREX was the achievement of the very small systematic error of 0.014 ppm. This strongly suggests that the total error can be significantly improved if more statistics can be obtained.

From Eq. 2 and references [33, 34], a number of physical quantities were deduced, specifically the form factor $F_W(q)$ of the weak charge density $\rho_W(r)$, the weak radius, a "weak charge skin", and ultimately the neutron skin

$$R_n^{208} - R_p^{208} = 0.33^{+0.16}_{-0.18} \text{ fm}. \tag{3}$$

This provides a (1.8σ) observation of the neutron skin in a heavy nucleus with a purely electroweak reaction. A second ^{208}Pb run called PREX-II has now been approved which has a proposed error in R_n^{208} smaller by a factor of three to ± 0.06 fm.

1.3 Nuclear Structure Physics and CREX

We now describe recent DFT and ab initio calculations for ^{48}Ca and how the direct test of these approaches by the proposed CREX measurement would constitute a major advance in nuclear structure physics.

1.3.1 Density Functional Theory Calculations

At the heart of nuclear DFT [3] is an energy density functional whose minimization yields the exact ground state energy and density of a nucleus. However, DFT does not provide a practical way to compute the functional. The commonly used EDFs are assumed to have a convenient form in terms of local nucleonic densities $\rho_p(r)$ and $\rho_n(r)$ and associated currents, involving perhaps a dozen free parameters, and these parameters are optimized [35, 36] to reproduce many nuclear observables. Using basic observables of stable nuclei, such as binding energies and charge radii, the optimization accurately constrains how the functional depends on the isoscalar density $\rho_0(r) = \rho_p(r) + \rho_n(r)$ and its gradient $\nabla\rho_0(r)$.

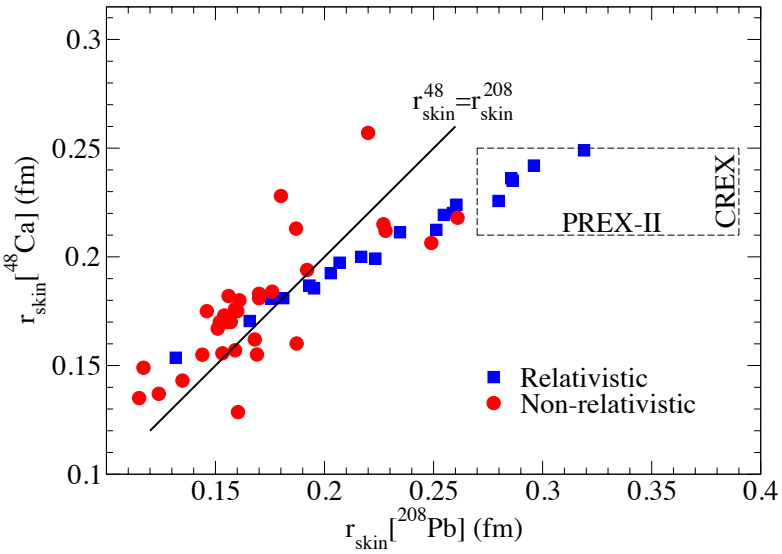

Figure 4: Predictions for $r_{\rm skin} = R_n - R_p$, from many non-relativistic and relativistic EDFs for ^{48}Ca vs ^{208}Pb. Also shown are projected error bands for the approved PREX-II experiment (± 0.06 fm, at the central value of the PREX result) and CREX (± 0.02 fm, at an arbitrary central value). (Based on Refs. [23, 37].)

However, there are not many well-measured isovector observables to accurately constrain how the functional depends on the isovector density $\rho_1(r) = \rho_n(r) - \rho_p(r)$ and $\nabla\rho_1(r)$. Isovector fields predicted by various functionals differ [37, 38]; hence, the predicted values for the neutron skin vary significantly. In Fig. 4 we show $r_{\rm skin}$ for ^{48}Ca that we abbreviate $r^{48}_{\rm skin}$ vs. $r_{\rm skin}$ for ^{208}Pb (abbreviated $r^{208}_{\rm skin}$) predicted by a variety of non relativistic (red circles) and relativistic (blue squares) density functionals. Remarkably, whereas all these models predict accurately the binding energy and charge radii throughout the nuclear chart, they are unable to agree on whether ^{48}Ca or ^{208}Pb has the larger neutron skin. For example, most of the non-relativistic

models displayed in Fig. 4 seem to suggest a larger neutron skin in ^{48}Ca than in ^{208}Pb ($r^{48}_{\rm skin} > r^{208}_{\rm skin}$). In contrast, most relativistic models predict the opposite ($r^{208}_{\rm skin} > r^{48}_{\rm skin}$).

The approved PREX II measurement of $r^{208}_{\rm skin}$, while relevant for astrophysics, does not fully constrain the isovector sector of the nuclear density functional. PREX II is critical in constraining the poorly known density dependence of the symmetry energy, particularly the parameter L that represents the slope of the symmetry energy at saturation density. There is a very strong correlation between L and $r^{208}_{\rm skin}$, so at present models with different values of L predict a large range of neutron skins in ^{208}Pb, ranging from less than 0.1 to greater than 0.3 fm (see Fig. 4). Thus, even the more accurate PREX II experiment may be unable to significantly constraint the isovector sector of the nuclear density functional.

However, once L is constrained by PREX II, DFT predicts a correlation between $r^{48}_{\rm skin}$ and $r^{208}_{\rm skin}$ that is testable with CREX. For example a large value of $r^{208}_{\rm skin}$ and a small value of $r^{48}_{\rm skin}$ is not expected with present EDF parameterizations. If PREX II and CREX were to yield such results, it would strongly suggest that present density functionals incorrectly model isovector contributions to the nuclear surface energy (for example gradient terms involving $\nabla\rho_1(r)$). These surface terms are much more important for ^{48}Ca than for ^{208}Pb because ^{48}Ca has a larger ratio of surface to volume. An additional attractive feature of ^{48}Ca, as compared to ^{208}Pb, is that the role of electromagnetic effects due to the Coulomb interaction is much reduced in the former system, thus allowing a cleaner study of nuclear isovector properties.

We emphasize that PREX II and CREX together will constrain isovector contributions to the nuclear EDF. **If PREX II and CREX results agree with DFT expectations***, this provides confidence in theoretical predictions of isovector properties all across the periodic table.* Apart from the inherent importance for nuclear structure physics, these predictions are important both for atomic parity experiments and for the extrapolation to very neutron-rich systems encountered in astrophysics.

If PREX II and CREX results disagree with DFT expectations*, this will demonstrate that present parameterizations of the isovector part of energy functionals are incomplete.* The current parameterizations are prone to large statistical and systematic errors related to isovector terms [6, 38, 39]. Locating and correcting this error is absolutely essential to develop the universal nuclear EDF that will be capable of extrapolating to very neutron-rich nuclei and bulk neutron-rich matter.

1.3.2 Ab initio coupled cluster calculations for ^{48}Ca

It is important to have a deeper understanding of energy functionals and to relate DFT results to underlying 2N and 3N interactions. Recently there has been considerable progress in ab initio coupled cluster calculations for medium mass nuclei [2]. Hagen *et al.* [40] have studied neutron rich calcium isotopes with large-scale coupled cluster calculations that take advantage of recent computational advances. These calculations provide a good description of ground and low lying excited states for a range of calcium isotopes [9].

In Fig. 5 we show preliminary results [41] for the proton, neutron, charge and weak densities of ^{48}Ca as predicted by the state-of-the-art coupled cluster calculations using recently-optimized chiral N2LO NN interactions [42] augmented by 3N forces. The corresponding radii are collected in Table 1. The calculations use a somewhat small model space when calculating the 3N force contributions. Therefore the results are still preliminary, even though the agreement with existing experimental data is quite good.

The effects of 3N forces on the neutron density is significant [43, 44, 45]. Therefore a measurement of $r^{48}_{\rm skin}$ will provide a very useful test of ab initio theory. Present theoretical uncertainties on the $r^{48}_{\rm skin}$ prediction

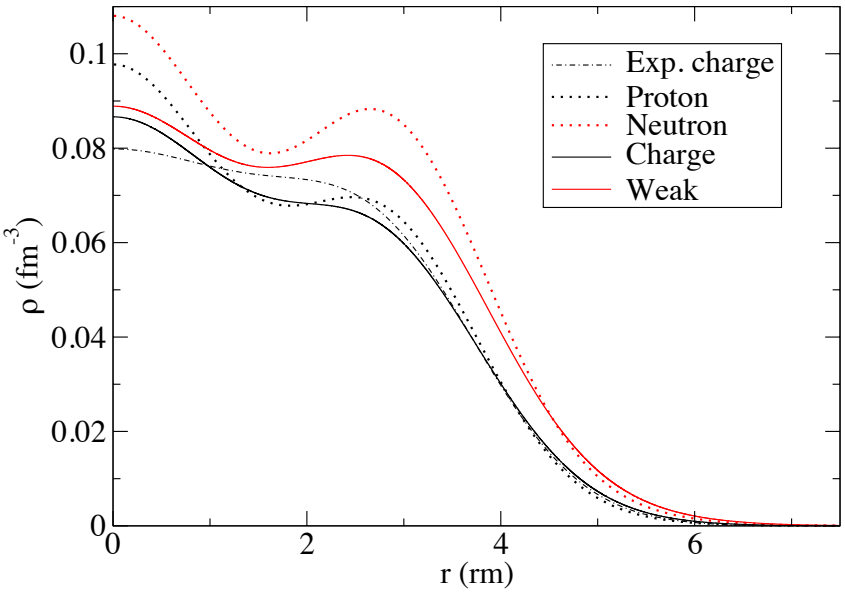

Figure 5: Preliminary microscopic coupled cluster calculations [41] for ^{48}Ca. The dot-dashed curve is the experimental Fourier Bessel charge density [47] , the theoretical charge density is the solid black curve while the weak charge density is the solid red curve. Finally the theoretical point neutron (proton) density is the dotted red (black) curve.

are large and include contributions from truncating the chiral expansion, the parameters of the 3N force, model space truncations in many body calculations, and omitted terms in the coupled cluster expansion. However the situation is improving rapidly as uncertainty quantification for nuclear structure calculations is an important subject that is receiving considerable attention [5, 42]. For example, More *et al.* have developed ways to minimize errors in calculated radii from model space truncations [46]. We expect accurate estimations from these ab initio calculations in the near future.

If CREX agrees with the results of coupled cluster calculations this provides a crucial test of ab initio nuclear structure theory that increases confidence in a variety of nuclear structure predictions and illuminates the role of three-nucleon and in particular three neutron forces. This is important for a variety of medium mass neutron rich isotopes that are presently being studied with radioactive beams. It may also be important for calculations of double-beta decay matrix elements. (The isotope ^{48}Ca is the lightest nucleus that undergoes double-beta decay and we expect microscopic calculations of double-beta decay matrix elements to be available first for ^{48}Ca.)

If CREX disagrees with these microscopic calculations, something is likely missing from present ab initio approaches. For example, the chiral expansion may not converge as well as hoped because of large Δ resonance contributions. This would significantly impact all nuclear structure theory.

Table 1: The radii (in fm) of ^{48}Ca obtained in preliminary coupled cluster calculation of Ref. [40]. Listed are the point proton R_p, neutron R_n, charge R_{ch} and weak charge R_W radii. Finally the experimental value of the charge radius R_{ch} (exp) is shown [48].

R_p	3.438
R_n	3.594
$R_n - R_p$	0.156
R_W	3.697
R_{ch}	3.526
R_{ch} (exp)	3.48

1.3.3 Summary of CREX Motivation

Within the next few years, R_n measurements on ^{208}Pb and ^{48}Ca along with measurements on the same nuclei of the electric dipole polarizability (α_D) [6], another well-defined and experimentally accessible isovector observable, will form a foursome of powerful experimental inputs to tune nuclear models of increasing sophistication. There is a model-dependent relationship between α_D and $r_{\rm skin}$ [37]. A measurement of α_D in ^{208}Pb [49] has been able to rule out models that predict either very small or very large neutron skins in ^{208}Pb. It is important to measure $r^{48}_{\rm skin}$ directly and independently to corroborate the connections between these observables and to further constrain the isovector sector of these models. Finally we note that an α_D measurement in ^{48}Ca is underway and data is presently being analyzed [50].

In summary, while PREX-II will provide a powerful and model-independent constraint on the density dependence of the symmetry energy (the parameter L), models predicting neutron radii of medium mass and light nuclei are affected by nuclear dynamics beyond L. CREX will provide new and unique input into the isovector sector of nuclear theories. In particular, the high precision measurement of R_n (± 0.02 fm) in a doubly-magic nucleus with 48 nucleons will provide a critical bridge between ab-initio approaches and nuclear DFT.

1.4 Transverse Asymmetry Measurements

A routine and mandatory part of a parity violation experiment is to spend about 1 day measuring the transverse asymmetry A_T in order to constrain the systematic error from a possible small transverse component of the beam polarization (section 2.7.4). The measurement of the A_T itself provides an interesting challenge for theoretical prediction, requiring calculation of box diagrams with intermediate excited states [51, 52].

For these ancillary measurements, the beam polarization is set normal to the electron scattering plane. For this configuration, the asymmetry follows an azimuthal modulation

$$A_T = A_n \vec{P} \cdot \hat{k} \tag{4}$$

where A_T is the transverse asymmetry, A_n is the amplitude of the asymmetry modulation, $\vec{P}$ is the polarization vector of the electron, and $\hat{k}$ is the unit vector of the cross product between the incoming and outgoing electron momentum vectors. This asymmetry is, in particular, a direct probe to multiple-photon exchange as it is vanishes in the Born-approximation by time reversal symmetry. The importance of understanding

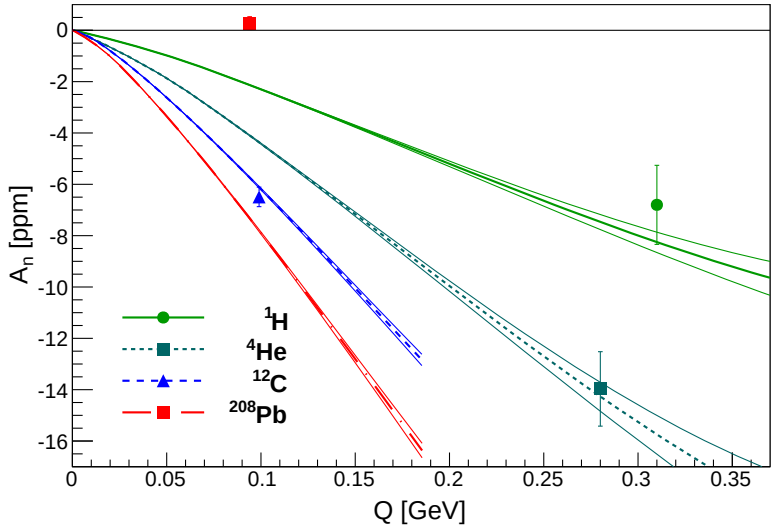

Figure 6: Extracted asymmetries A_n vs. Q for several different nuclei [52].

two-photon exchange, for example, has been highlighted by the discrepancy between G_E^p measurements using Rosenbluth-separation and polarization observables [53].

Theoretical predictions are challenging to calculate due to the contributions from hadronic intermediate states in $\gamma - \gamma$ box diagrams and Coulomb distortion effects which are present for large Z. However, predictions have been made that these are on the order of a few ppm with beam energies of 1-2 GeV and $\theta_e \sim$ few degrees using the optical theorem with photoabsorption data [51] to describe the intermediate states. Different approaches, such as using generalized parton distributions to describe $e - p$ data [54], have also been taken.

Data for these asymmetries with ^{1}H, ^{4}He, ^{12}C, and ^{208}Pb have been published by our collaboration [52] and are shown in Fig. 6. There is significant disagreement from theory in ^{208}Pb, the sources of which are not presently well understood and motivate more measurements at intermediate Z, as well as new calculations that involve simultaneously Coulomb distortions and dispersion corrections. In light of this motivation, the CREX experiment measurements on ^{48}Ca could be useful to help elucidate the dependence of these asymmetries on Z and Q^2 by providing an additional data point. Because this asymmetry is so small, directly measuring it requires PV-type precision for which this experiment is designed. A precision of ~ 0.5 ppm would be on similar grounds as the previous data and would require significantly less running time than the proposed parity-violating measurement.

Table 2: Comparison of the 2005 HAPPEX-II experiment, the planned PREX-II measurement, and the CREX measurement proposed here.

	HAPPEX-II	PREX-II	CREX
Energy	3.1 GeV	1.0 GeV	2.2 GeV
Angle	5.7 degrees	5 degrees	4 degrees
A_{PV}	1.4 ppm	0.6 ppm	2 ppm
rate	100 MHz	1 GHz	100 MHz
A_{PV} precision	7%	3% (proposed)	2.4%

2 Experimental Setup

2.1 Overview

The methods required for this measurement have been successfully used in PREX [33] and HAPPEX [55]. The significant new apparatus elements for this proposal are the ^{48}Ca target and a new septum magnet. The rest of the apparatus is standard equipment. The experiment is designed for $150\ \mu$A pass (2.2 GeV) beam. Table 2 highlights the experimental configuration and goals of this proposal relative to recent parity violation experiments in Hall A. Because of larger transverse asymmetries which are a potential systematic in this measurement, we cannot run this experiment if the beam is not fully longitudinally aligned to minimize transverse polarization.

Longitudinally polarized electrons scatter elastically from an isotopically pure ^{48}Ca target into the HRS (high-resolution spectrometers) in Hall A. To reach a 4° scattering angle, septum magnets are placed upstream of the HRS. The scattered electrons are detected by a calorimeter placed in the focal plane of the HRS, positioned to isolate the elastic peak and discriminate against inelastic levels. The electrons are integrated over each helicity window (R and L helicity) and an asymmetry is formed $A = \frac{\sigma_R - \sigma_L}{\sigma_R + \sigma_L}$.

We also plan on doing a measurement where the beam is polarized vertically-transverse (i.e. perpendicular to the electron scattering plane) at the same kinematics. The value of the asymmetry is not well known as discussed in Section 1.4, but to achieve a statistical uncertainty of 0.4 ppm, will require about two shifts of running at $150\ \mu$A.

2.2 Septum Magnet

The septum magnet will be a warm septum magnet similar to what was successfully used during PREX. A higher current density will be required, because the beam energy is 2.2 GeV (compared to 1.05 GeV) and because the scattered electron angle will be 4°. The two main issues when designing the septum are the hardware resolution and the acceptance. One needs sufficient hardware resolution to select the elastic peak with an integrating detector while discriminating the inelastic levels (the lowest level is 3.8 MeV for ^{48}Ca). In order to achieve a 4° angle, the scattering chamber will need to be moved back ~ 45 cm, which will reduce the solid angle. To achieve a good hardware resolution one needs a nearly pure dipole magnetic field with small higher-order multipoles. The solid angle should be as large as possible, given the constraints on scattering angle and hardware resolution. Figure 7 shows the hardware resolution effects for the separation of the first excited state at 3.84 MeV from the elastic peak.

Because of damage to the old coils, new (identical) coils will have to be constructed for PREX-II.CREx plans to use the two-coil configuration which was designed to improve the optics for PREX-II, Fig. 8, but with a higher current density ($\sim$1350 A/cm^2) in order to achieve the necessary field integral.

While this is an aggressively large current density, we note that it is smaller than that proposed for the MOLLER spectrometer coils, which has been subjected to an internal review by magnet experts. We plan to apply the lessons from those studies in designing new coils for this proposal.

The main concern is the size of the water-cooling hole; it needs to be large enough to avoid developing blockages due to erosion by the high flow velocity of the water. The current septum coils have a water-cooling hole twice as big as the smallest recommended hole size, so new coils with the same conductor will be adequate. A new power supply to drive the higher current, as well as additional LCW pumps (to achieve the necessary water flow to cool the coils) will be necessary.

Using the TOSCA model for the two-coil septum at $\theta = 4^\circ$ we have generated the transport functions for the septum and HRS optics combination, and have use this in a full simulation of the spectrometer acceptance leading to more accurate estimates of the rates, and acceptance-averaged asymmetries, sensitivity to neutron radius, and statistical errors presented in section 2.5. The solid angle of 2.9 msr is larger now than assumed in the 2012 proposal.

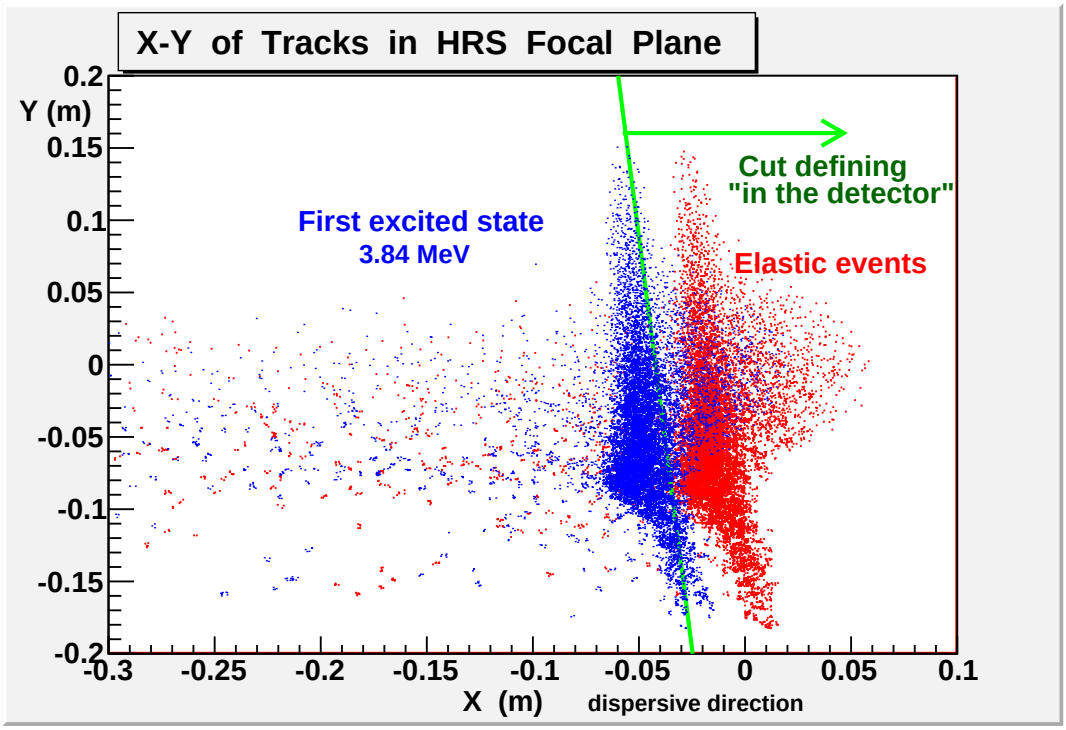

Figure 7: Simulated positions in the focal plane for the elastically scattered events (red) and events from the first excited state (blue). The first state has a cross section that is 0.94% of the elastic, and the placement of the detector shown suppresses this to a 0.19% background. The first ten inelastic states [60] add to a 0.4% background.

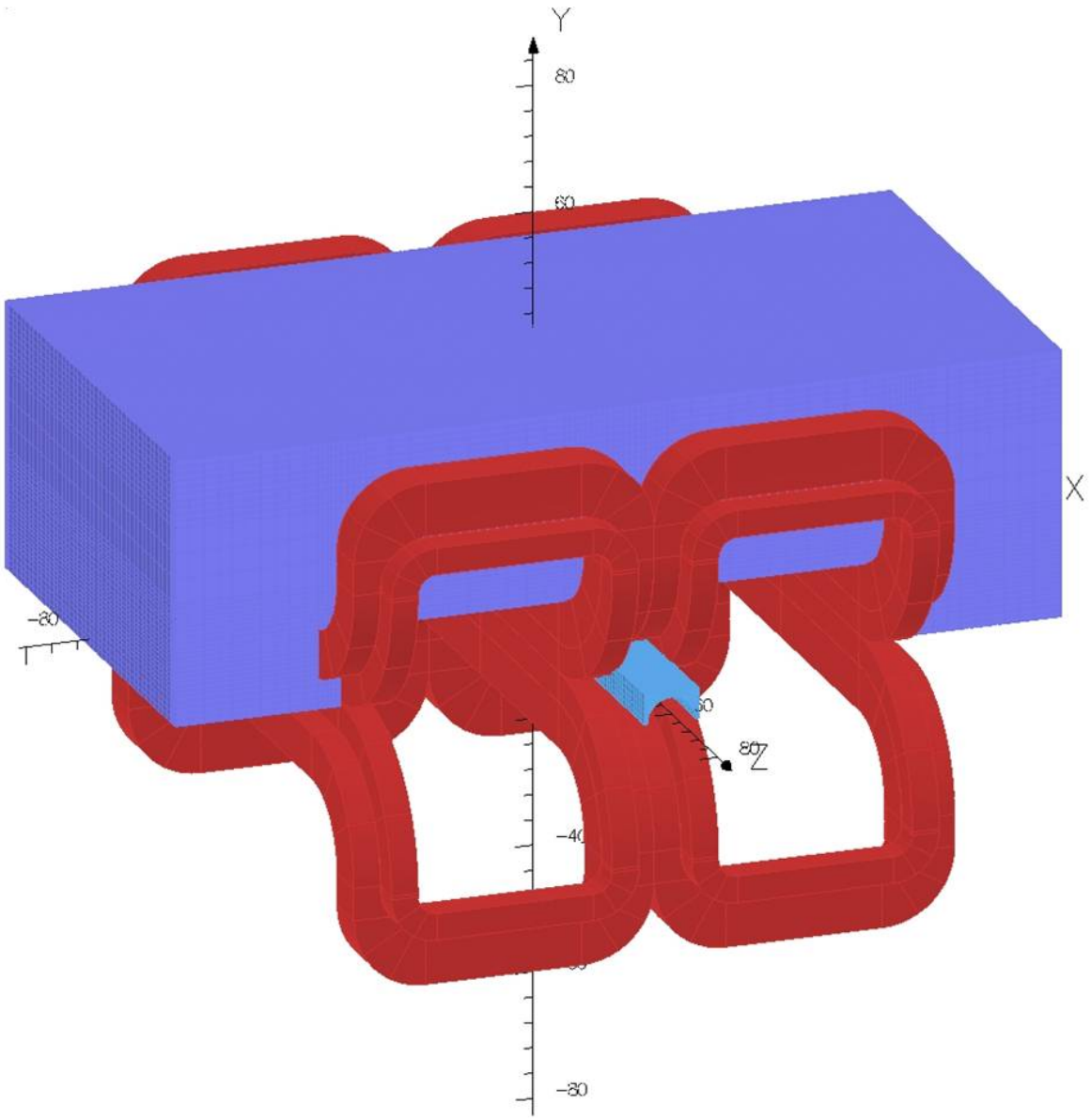

Figure 8: TOSCA picture of the two coil septum.

2.3 Calcium Target

The calcium target will be a 1 gm/cm^2 isotopically pure ^{48}Ca target. Such a target was deployed in Hall A in the Spring of 2011 for the E08-014 experiment, where it ran for several days of beam at 40μA. We are proposing to run at 150 μA. Thermal calculations show that with a standard raster pattern to distribute the heat from the beam, the target temperature will not exceed 120°C (the melting point is 842°C) if we can keep the temperature on the border of the target fixed at room temperature.

The target design concept is shown in Fig. 9. The entire assembly weighs under 60 lbs and fits inside our standard target chamber. The ^{48}Ca slab is housed in a vacuum chamber with thin entrance and exit ("end-cap") windows. This chamber traps the atoms in case the target is destroyed, which is important since ^{48}Ca is extremely expensive but can be recovered if the atoms are captured. This target design is similar to the one used during the E08-014 experiment (see Figs. 11 and 12) except that this proposal calls for a longer target housing to allow electrons scattered from the ^{48}Ca at angles near to 4° to clear the blockers located at the front and exit thin windows. The blockers are $\sim$4 mm thick, 27 cm long cylinders and serve two purposes: (a) to energy-degrade electrons that scatter from the end-cap windows so they don't contribute as background in the integrating detectors in the HRS focal plane; and (b) cryogenic cooling running through tubing on the blockers will carry away the 270 Watts of beam heating, thus cooling the ^{48}Ca slab as well as the entrance and exit windows.

The end-cap windows need to be thick enough to withstand 1 atm pressure differential prior to being installed in the scattering chamber; during beam delivery, however, there will be no pressure difference since the scattering chamber is evacuated. At the same time, the end-caps must be thin enough to not create excessive background and to limit multiple scattering effects for the initial beam on target and for the beam transport to the dump. Similarly, the windows for accepted tracks should not contribute significant multiple scattering. Assuming stainless steel windows, a thickness of $\sim$0.3 mm appears to be a practical compromise. The beam pipe in the blockers is about 1 inch inner diameter (in our simulations we used 2.54 cm upstream and 2.0 cm downstream), sufficient to deliver the beam through it. In order to clear the trajectories downstream while using a standard 4×4 mm^2 raster with an assumed 1 mm misalignment, the downstream blocker is tapered as shown in Fig. 9. Electrons that scatter from the end-caps and pass through the blockers will lose typically ≥ 20 MeV by ionization loss through the material, and hence will not hit the detectors. In the past year, we have run Geant4 simulations of the target region to confirm that the background from the end-caps reaching our detector will be negligible because of this energy loss and the heavy suppression by the HRS spectrometers. Some typical events are shown in Fig. 10. The simulations have led to a more optimized geometry presented here. Some further optimization may be possible to allow for a bigger beam clearance; alternatively, we may need to have a fast shutdown on beam position excursions to avoid hitting the blockers with beam.

The thermal calculations assumed that the edge of the ^{48}Ca slab is held at room temperature (however, present plans are for a cryogenically cooled design); this might not be the case; however, there is a lot of headroom on these calculations. What's more, beam tests are planned with a non-isotopically enriched calcium target during an earlier experiment such as PREX-II to verify that the target remains stable under operation at 150 μA.

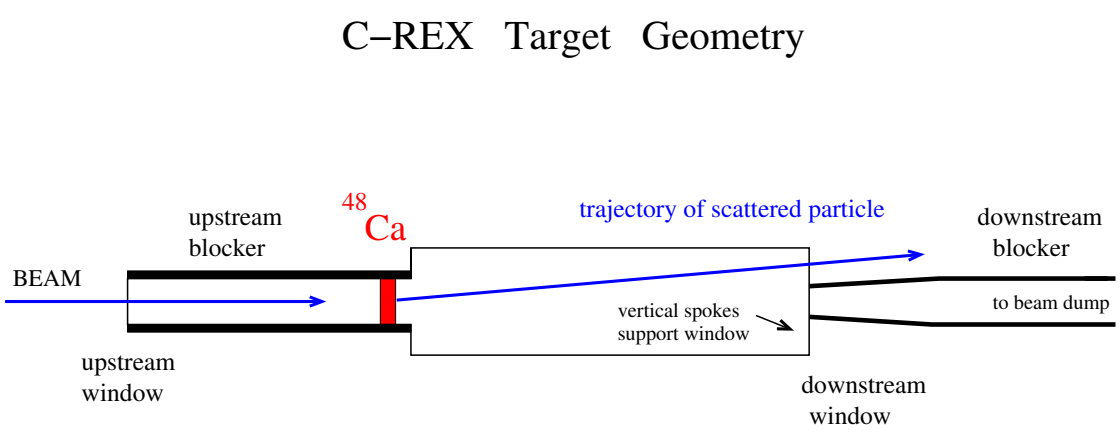

Figure 9: Conceptual drawing of the proposed ^{48}Ca target design. A 1 gm/cm^2 thick isotopically pure ^{48}Ca target is housed in a vacuum chamber. The chamber traps the atoms in case the target is destroyed. This is similar to the target used during the E08-014 experiment (see Figs. 11 and 12) except that the design here calls for a longer target housing with blockers on the entrance and exit windows to energy-degrade electrons that scatter from those windows, and with cryogenic cooling applied to the blocks to carry away the 270 Watts of heat from the beam.

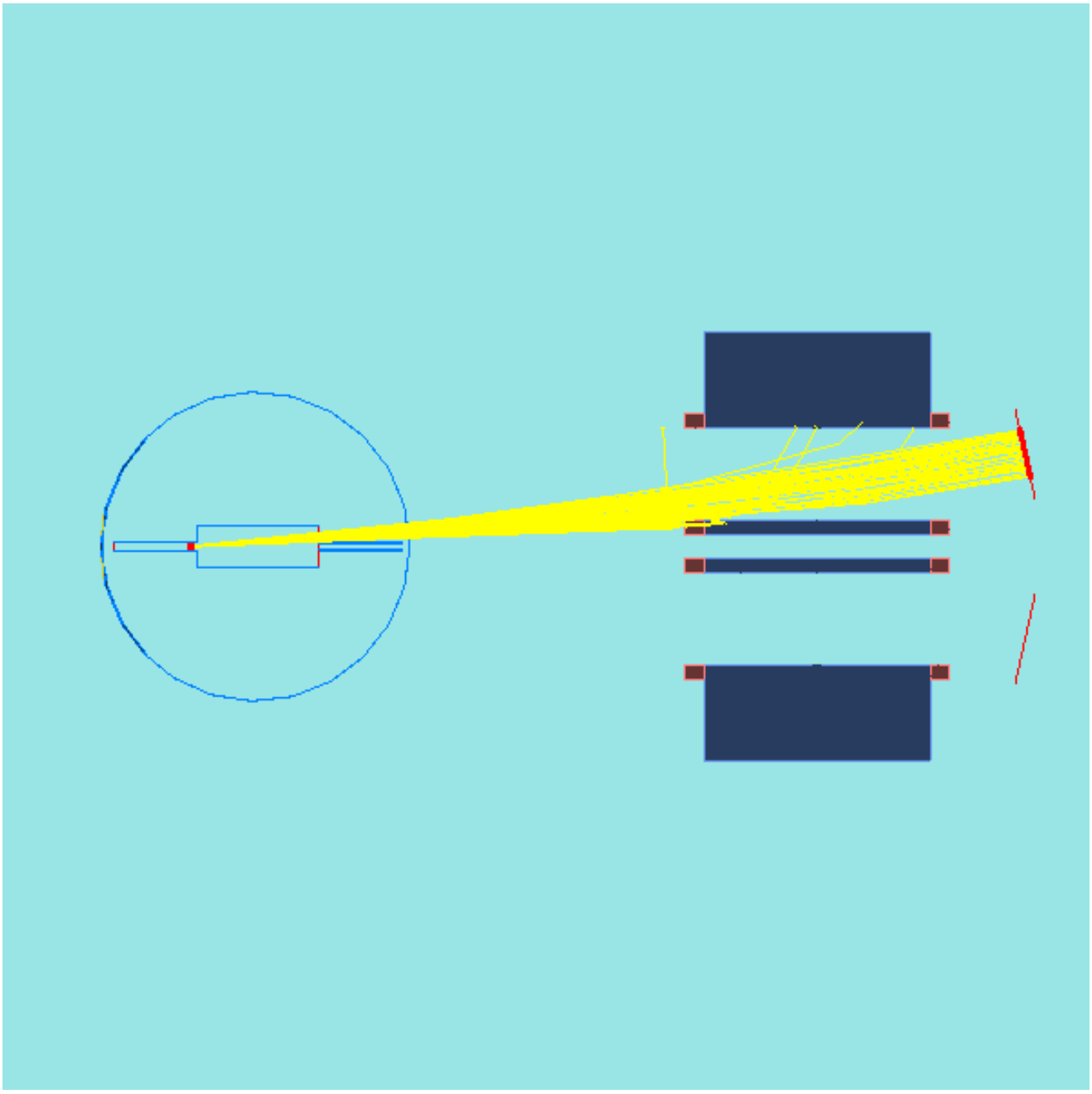

Figure 10: Typical Geant4 events from the proposed ^{48}Ca target. Events were also simulated from the two end-cap windows (not shown here) to verify the low background from these as a result of energy degradation in the blockers, as well as to optimize the geometry.

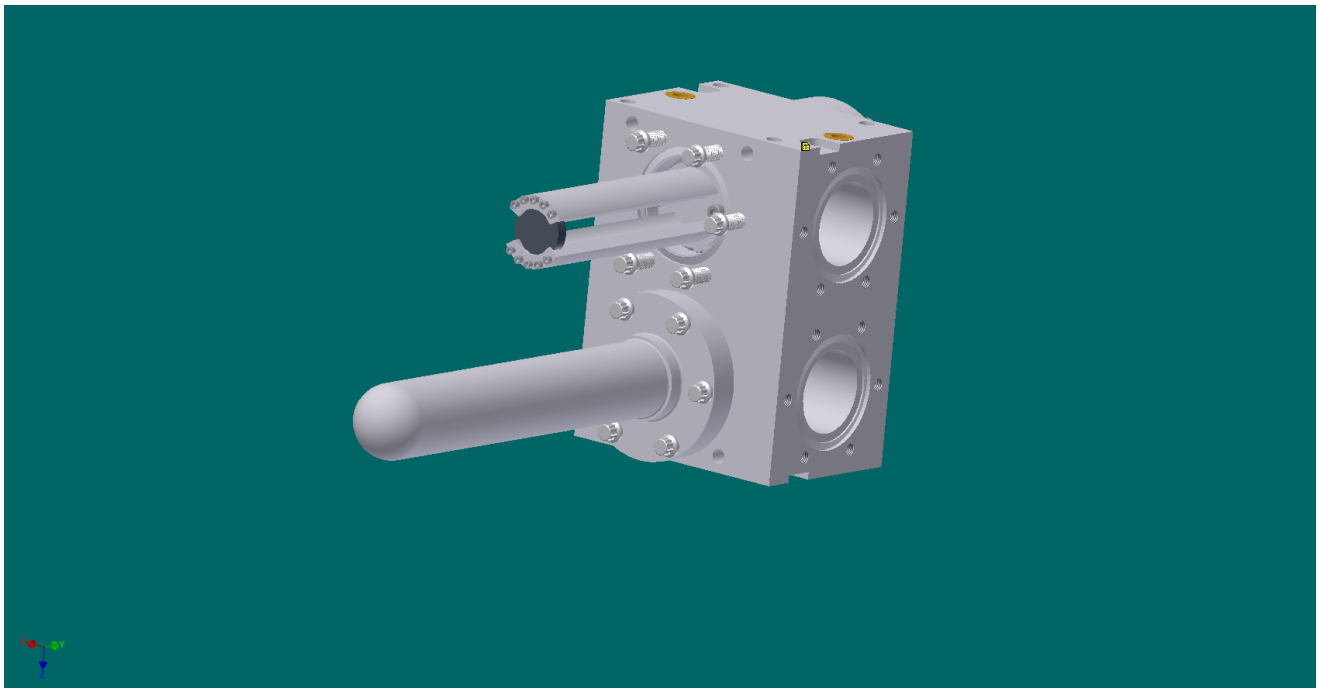

Figure 11: 3D view of the existing calcium target that has been used in Hall A during experiment E08-014. For that experiment, two targets were mounted on one block. The picture shows one target with the inner part exposed. The two targets used were ^{40}Ca and ^{48}Ca. For CREX, this target will be modified significantly as in Fig. 9. It will be longer and there will be blockages on the entrance and exit windows to energy-degrade electrons from them so they don't reach the detector.

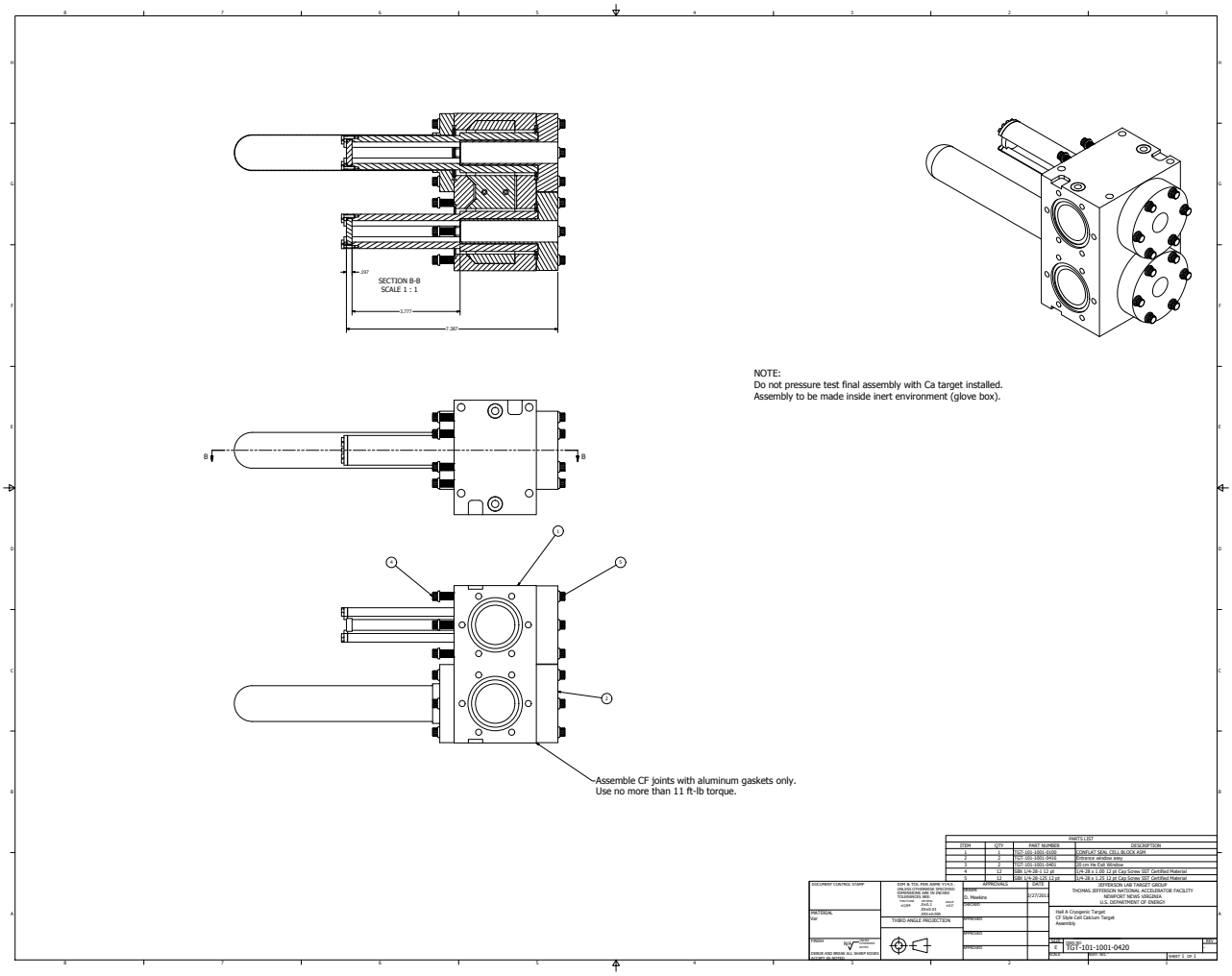

Figure 12: Engineering drawings of the existing ^{48}Ca target used during E08-014. See the figure caption for Fig. 11.

2.4 Detectors

The integrating electron detectors will be similar to those used in PREX, where quartz will be used to detect Cerenkov photons. These will be connected to PMTs and the signal will be integrated in an existing data acquisition system previously used in other parity experiments and designed for its high linearity.

To minimize the size of the detectors which improves the light collection, a special optics tune for the spectrometers will be used which focuses the elastically scattered electrons into an area of several square centimeters. This area is above the vertical drift chambers by about a meter and the detectors will be mounted on a remotely controllable movable stand. This allows us to optimize the placement of the detectors with beam on target.

The collaboration has the experience of building these detectors from PREX. The design can be directly translated to this one by increasing the length of quartz to $13\ \mathrm{cm}$ based on optics simulations. We anticipate performance from the detectors comparable to that seen in the PREX measurement.

While a quartz Cerenkov detector is valued for radiation hardness and insensitivity to soft backgrounds, there is a particular challenge for few GeV electrons. In this energy range, shower fluctuations in a thick or radiated detector significantly degrade energy resolution, while photon statistics degrade the energy resolution for a thin detector. The energy resolution ΔE at nominal electron energy E increases the statistical error that one would have with infinite resolution σ_0 to obtain the total statistical error $\sigma = \sigma_0\sqrt{1+(\frac{\Delta E}{E})^2}$. Based on experience in the PREX experiment, we expect an reduction of statistical precision of a factor of 1.06 due to detector resolution.

2.5 Kinematics Choice

The optimum kinematics of the experiment is the point which effectively minimizes the error in the neutron radius R_n. This is equivalent to maximizing the following product, which is the figure-of-merit (FOM) for this technique of neutron-density measurement: FOM = $R \times A^2 \times \epsilon^2$, where R is the scattering rate, A is the asymmetry, and $\epsilon = \frac{dA/A}{dR_n/R_n}$ is the the sensitivity of the asymmetry for a small change in R_n. Here, dR_n/R_n is a fractional change in R_n and dA/A is a fractional change in A.

Using the high-resolution spectrometers (HRS) of Hall A, a small scattering angle maximizes the FOM. Given practical constraints on how low an angle (4°) we can reach with septum magnets, the energy is fixed and turns out to be 2.2 GeV, which is a natural 1-pass beam energy for CEBAF operations in the 12 GeV era.

To evaluate the FOM we used the "Hall A Monte Carlo" (`hamc`), a simulation framework which has been used for three previous parity experiments. It models the acceptance of the HRS and septum and allows for averaging quantities such as the asymmetry over the acceptance. The acceptance for the spectrometers was modeled by Snake transport functions which were fitted to the TOSCA field map of the septum magnet, combined with the known transport for the HRS. The solid angle is 2.9 msr for each HRS.

The differential cross section, the asymmetry, and the sensitivity of the asymmetry on the neutron radius for $^{48}\mathrm{Ca}$ was supplied by C. J. Horowitz [56] which was calculated by numerically solving the Dirac equation and therefore includes Coulomb distortion effects. Radiative losses are included by following the prescription by Mo and Tsai for nuclei [57]. The simulation also includes multiple scattering and ionization energy

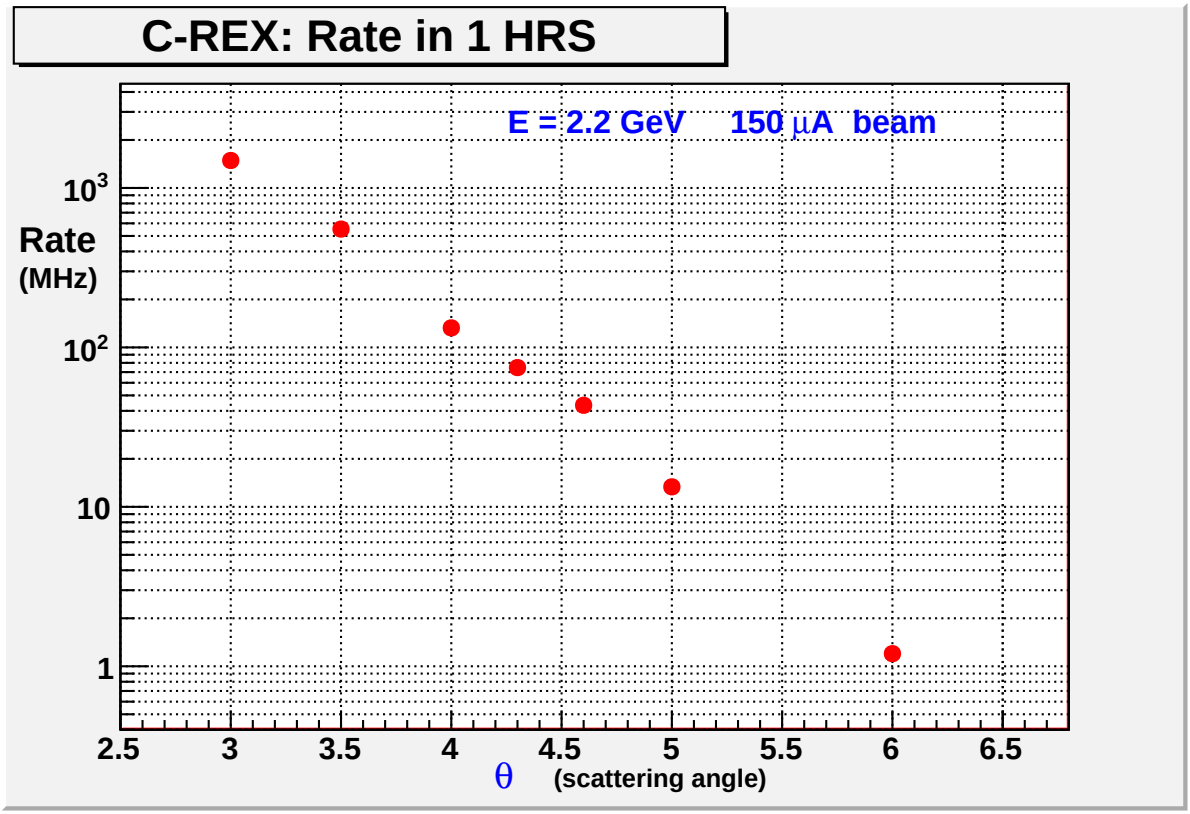

Figure 13: Acceptance-averaged rates for 1 HRS versus central angle for 2.2 GeV at 150μA.

loss. The accepted rate is reduced by a factor of 2.7 due to the finite moment acceptance of the detector. This factor also includes an empirical correction to the simulation estimate based on observation during the PREX-I measurement, which used at 10% radiator.

For running conditions, a beam current of 150 μA with energy 2.2 GeV and 85% polarization and a 5% radiation length (1 g/cm^3) target was assumed. As described above, the statistical errors in the asymmetry were inflated by a factor of 1.06 due to the energy resolution of the detectors. A running time of 35 days was used with no considerations for downtime. In Figs. 13, 14, and 15 the rate, measured asymmetry, and asymmetry sensitivity to the neutron radius is plotted against scattering angle, averaged over the range of acceptance. The error in the neutron radius, Fig. 16, is minimized where the FOM is maximized. A 1.2% assumed systematic error changes the optimum FOM kinematics, as noted in the figure.

2.6 Polarimetry

The Compton and Møller polarimeters in Hall A will together be able to achieve better than 1% accuracy in beam polarization during the run. Improvements in polarimetry will continue during the approved PREX-II experiment and are of vital importance to the entire future Hall A program. In particular, due both to the relative higher energy and recent technical advances, the Compton polarimeter will have a higher figure-of-merit and lower systematic errors than during PREX.

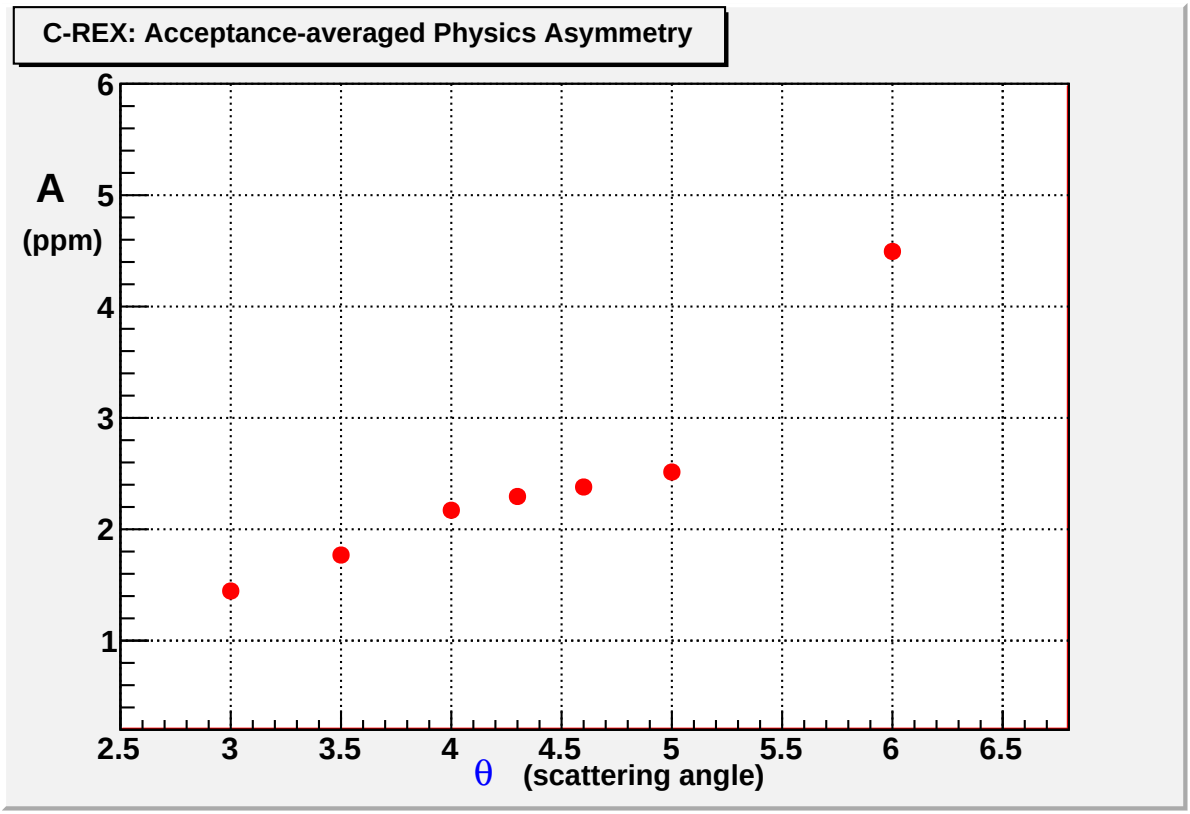

Figure 14: Physics asymmetries versus central angle for 2.2 GeV. To get the raw asymmetry one would need to multiply by 0.85 for the beam polarization.

2.6.1 Møller Polarimeter

In 2009 - 2010, the Møller polarimeter was upgraded as follows: 1) The "brute force" polarization of the target foil using a strong (3T) magnetic field, as has been done in Hall C [58]. Also the target has a smaller thickness and lower heating; 2) A segmented aperture detector to accommodate the higher rates; and 3) A new fast DAQ based on Flash ADCs to handle the higher rates with smaller deadtime and to provide more information about the events such as pileup. Table 3 shows the systematic errors achieved during PREX which totaled 1.1%. A significant correction due to the Levchuk effect was required in this measurement. This was related to operation at low beam energy, for which the standard optics of the quadrupole spectrometer introduced a hard acceptance cut-off due to the limited beam-pipe aperture. This effect will be lessened at 2.2 GeV, and systematic error due to the correction can be better controlled through careful characterization of the acceptance. With this improvement, and other incremental improvements, a systematic error of 1% is expected to be achieved during the CREX measurement.

2.6.2 Compton Polarimeter

The Compton polarimeter was upgraded in 2009 - 2010 to achieve an improved figure of merit at low energies by using a new green laser and resonant cavity. The signals from back-scattered photons were integrated in custom Flash ADCs. This integration technique eliminated the systematic error from thresholds that affected the older counting method. For PREX, the total systematic uncertainty totaled 1.2%, a major

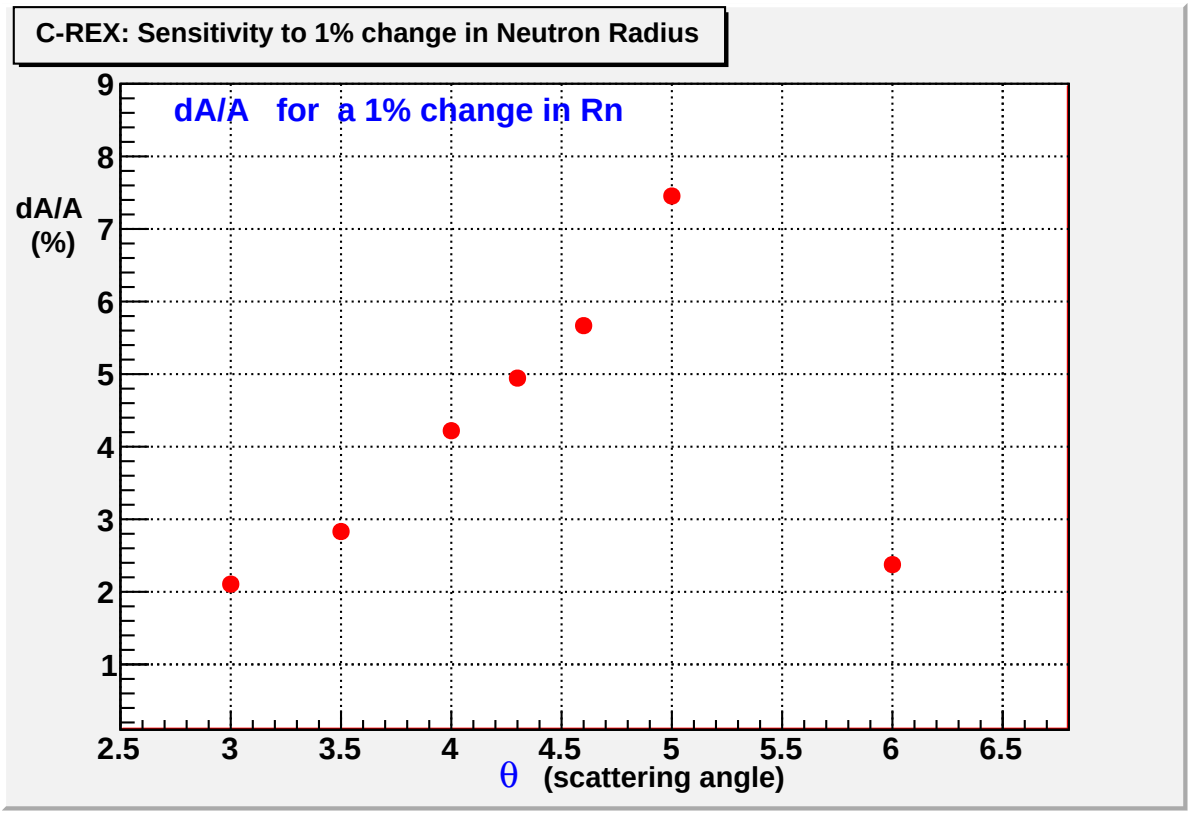

Figure 15: Sensitivity of the asymmetry to a 1% change in R_n versus central angle for 2.2 GeV.

accomplishment for 1 GeV running. At the 2.2 GeV beam energy of this proposal, the Compton Polarimeter will operate with higher statistical figure-of-merit and increased resolution of the scattered photon spectrum. The Compton polarimeter results for the HAPPEX-III experiment [59], with a relative systematic error of 0.9% at 3.4 GeV, are likely a better guide for expected systematic errors during CREX. For HAPPEX-III, the systematic error was dominated by a 0.8% uncertainty in laser polarization. New techniques for the control of this uncertainty have been developed during on the Hall C Compton polarimeter during the Qweak experiment. These will be applied in Hall A and can be expected to reduce the photon polarization uncertainty to the level of 0.2%.

Table 4 shows the estimated systematic errors for CREX, based on those achieved during PREX and HAPPEX-III and accounting for the expected improved knowledge in laser polarization. Based on these estimates, the uncertainty in beam polarization for the CREX should be not worse than 0.8%.

2.7 Systematic Errors

The total systematic error goal is about 1.2% on the asymmetry, compared to an anticipated statistical accuracy of 2.1%. The dominant contributions are all from effects which have been well understood in previous experiments [33, 55].

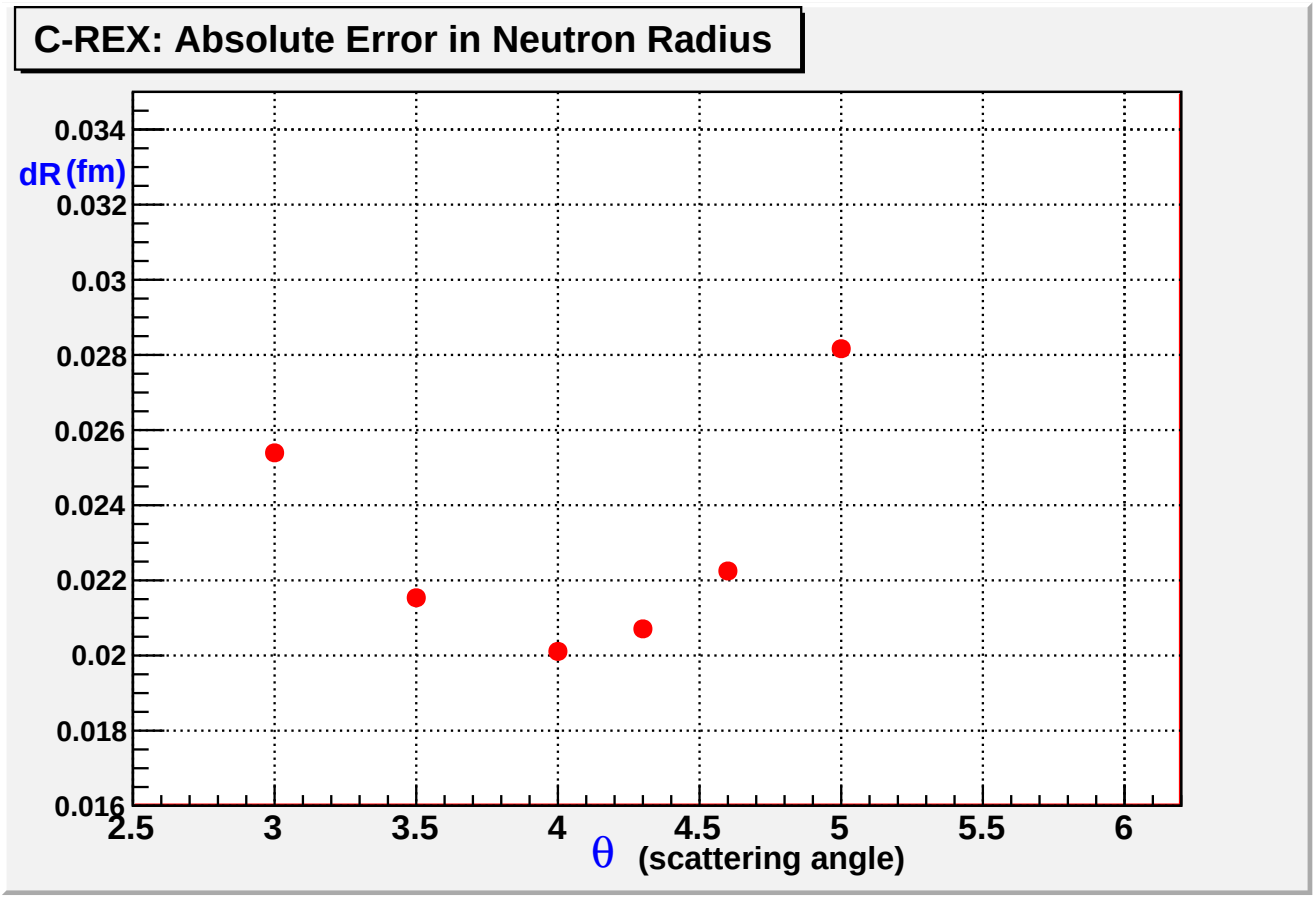

Figure 16: Error in R_n versus central angle for 2.2 GeV (1-pass beam) for 35 days at 150μA for a target thickness of 5% radiation length. An error of 0.02 fm is feasible. A 1.2% systematic error was assumed. The optimal angle is 4°.

Table 3: Møller Polarimeter Systematic Errors during PREX. In particular the uncertainty due the Levchuk effect should be reduced significantly for the CREX measurement.

Iron Foil Polarization	0.25%
Targets Discrepancy	0.5%
Target Saturation	0.3%
Analyzing Power	0.3%
Levchuk Effect	0.5%
Target Temperature	0.02%
Deadtime	0.3%
Background	0.3%
Other	0.5%
Total	1.1%

Table 4: Anticipated Compton Polarimeter Systematic Errors for CREX

Laser Polarization	0.2%
Gain Shift	0.7%
Collimator Position	0.02%
Nonlinearity	0.3%
Total	0.8%

Table 5: Systematic Error Contributions in CREX

Charge Normalization	0.1%
Beam Asymmetries	0.3%
Detector Non-linearity	0.3%
Transverse	0.1%
Polarization	0.8%
Inelastic Contribution	0.2%
Q^2	0.8%
Total	1.2%

2.7.1 Beam Induced Asymmetries

At the end of 6-GeV era parity running, PREX was able to achieve overall asymmetry corrections due to helicity-correlated beam position fluctuations of about 40 ppb with position differences < 4 nm. The position/asymmetry correlations are corrected in the measured asymmetry using two independent methods: first, directly observing the asymmetry correlations by the natural beam motion and second, by systematically perturbing the beam through a set of magnetic coils (dithering). Achieving these small values was possible in part by periodically inserting the half-wave plate and the injector and flipping the helicity of the beam using a double-Wien filter which helps them cancel over time.

The correction made was dominated by fluctuations in the beam intensity due to small changes in the accepted angle and the sharply falling lead cross section. As we are at higher Q^2 (0.022 $(\mathrm{GeV/c})^2$) and ^{48}Ca is a smaller nucleus, $d\sigma/d\theta$ is smaller by a factor of six. We will conservatively assume that the uncertainty on the corrections we apply will be 7 ppb, the same as PREX.

The integrated signals in the helicity windows are normalized to the beam current monitor signals to remove helicity correlated beam intensity fluctuations. Non-linearities in the BCMs produce additional false asymmetries, which are related to the overall charge asymmetry. Based on past running, we can expect an cumulated charge asymmetry less than 100 ppb and an uncertainty on that correction of 1.5%, so 1.5 ppb, or 0.1% propagated to the final asymmetry.

2.7.2 Inelastic Contributions

The first few inelastic excited states were simulated with the appropriate strengths by using fits to form factor measurements of electron scattering from ^{48}Ca done at MIT-Bates [60]. These measurements covered the same momentum transfer range of interest here.

Elastic and inelastic events were simulated using our transport model for the HRS with 2-coil septum mag-

net, Fig. 7. The first excited state at 3.84 MeV has a cross section that is 0.94% of the elastic cross section, and the placement of the detector shown suppresses this to a 0.19% background. The next most important contribution is the second excited state (4.51 MeV, contributing 0.18% background). Altogether, the first ten inelastic states produce a 0.4% background. This might be further reduced with fine-tuning of the spectrometer optics and detector geometry.

Calculation of the contributing asymmetries is underway, but they are not expected to be significantly different from the measured asymmetry. Assuming this, and assuming calculations are reliable to within 50%, this corresponds to a 0.2% systematic uncertainty with the presently estimated contamination. The contamination will also be measured during the experiment using the standard detectors and counting-mode DAQ.

2.7.3 Q^2 Measurement

For the kinematics of the experiment, the change of the asymmetry with respect to the electron scattering angle is sufficient such that our ability to measure the angle contributes to an effective uncertainty in the asymmetry. For ^{48}Ca at 4° with 2.2 GeV beam, $dA/dQ^2 \sim 60\ \mathrm{ppm/GeV^2}$, or $40\ \mathrm{ppm/rad}$.

To measure the scattering angle, survey techniques will be insufficient to constrain the propagated uncertainty to less than 1%. By utilizing a proton target and comparing the energy difference between the elastically scattered electron peak and the elastic peak from a heavier nucleus, the absolute angle can be fixed. Such a technique was used for PREX and obtained an angle resolution of about 0.4 msr. Given comparable energy resolution (after optics calibration), and taking into account the kinematic differences, a similar absolute angular resolution can be achieved for this experiment. This corresponds to an 0.8% uncertainty in the measured asymmetry.

Additionally, the relative acceptance of the spectrometers must be measured so the asymmetry, integrated over the acceptance, can be related to an effective Q^2. Periodically through the experiment dedicated Q^2 runs will be taken at a low beam current (~ 100 nA) which allows for the vertical drift chambers to be operated and provide high resolution event-based tracking.

2.7.4 Transverse Asymmetry

If the beam has a transverse component of polarization, a parity-conserving asymmetry is introduced into the spectrometers with an azimuthal modulation. By running both spectrometers symmetrically and summing over the signals, this component will largely cancel. However, the parity-conserving value is typically larger than the parity-violating and may be a potential contamination if the spectrometers are place asymmetrically.

The value of the transverse asymmetry from ^{48}Ca is presently poorly constrained by theory (as discussed in Section 1.4), but has been measured at similar Q^2 points for several nuclei, Fig. 6. A realistic estimate is that it will be about 8 ppm, or about 4 times larger than the proposed measured asymmetry.

To control this potential systematic, we plan to measure this asymmetry directly during the experiment to a statistical precision of 0.4 ppm and place collimators which are aligned to symmetrize the acceptance. If the collimators are placed vertically within 1 mm of the ideal positioning, the asymmetry is suppressed by a factor of 100. If the beam polarization is longitudinally oriented to within 2° then the transverse asymmetry is suppressed by another factor of 30. Because the asymmetry is only a factor of 4 larger, the overall

change in the asymmetry is suppressed to about 10^{-3}, and therefore a small contribution to the systematic uncertainty.

3 Radiation in the Hall

PREX-I suffered from radiation damage of equipment in Hall A which caused down-time for the experiment to repair electronics, as well as damage to soft O-rings that were used in the vacuum system downstream of the target. These problems and their mitigation are described in the PREX-II proposal [61]. In particular, we plan to make improvements to the radiation-shielding and to use hard metal seals for the vacuum chambers.

For the present proposal, we have computed with Geant4 the power from neutrons, photons, and electrons from the target and collimator. The most damaging component during PREX-I was the neutrons produced in the hall by electrons which were elastically scattered from the target. In order to mitigate this for PREX-II, the collimator bore will be reduced so that most electrons which would not reach the beam dump are intercepted by the collimator. This isolates the source of neutrons, allowing polyethylene shielding around the collimator region to contain the neutron flux. This combination of improved beamline collimation and neutron shielding has been shown to provide an order of magnitude reduction in the radiation level.

For ^{48}Ca the power from neutrons per incident electron from the collimator region is a factor of 10 less than expected for PREX-II (see Fig. 17). This is primarily due to the higher beam energy, for which a larger fraction of elastically scattered electrons are transported to the beam dump without requiring collimation. While the shielding configuration can still be optimized for the CREx configuration, it is clear that radiation in the hall can be held to levels significantly below those in PREX.

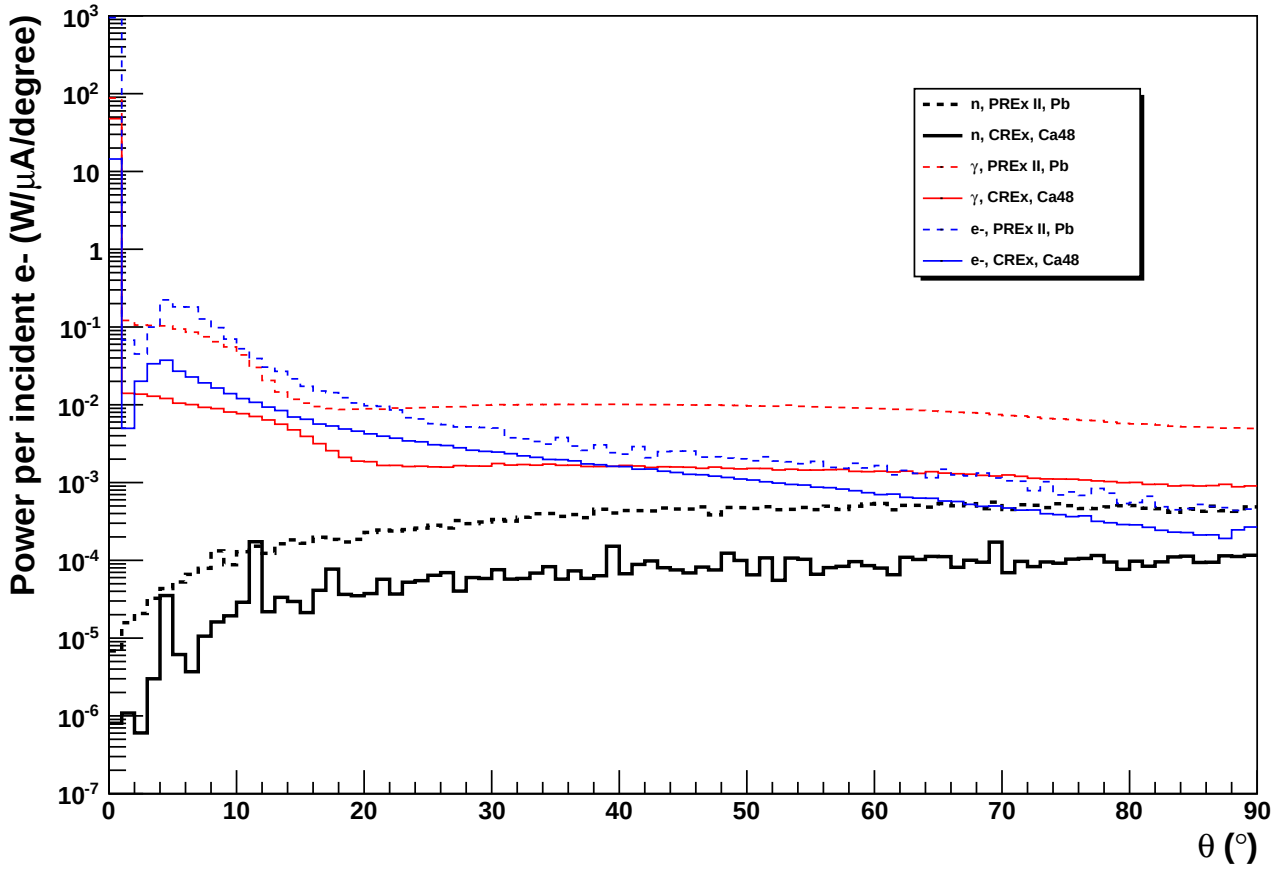

Figure 17: Plot of the power of particles from the target and collimator as a function of angle incident on a sphere centered on the target. The power from each type of particle - neutrons (black), photons (red) and electrons (blue) is compared between PREx II (dashed lines) and CREx (solid lines), with the appropriate target, collimator and energy. The dip in the electron and photon plots is because of the presence of the collimator; the entrance to the beam dump is $\sim 1^\circ$, so above this angle the power would be incident in the hall somewhere. Most of the neutrons originate in the collimator itself. The power from neutrons and photons (per μA) for CREx is about an order of magnitude smaller than PREx.

Table 6: CREX Proposed Data

Measured Asymmetry ($p_e\ A$)	2 ppm
Beam Energy	2.2 GeV
Scattering Angle	4°
Beam Current	150μA
Statistical Uncertainty of A_{PV}	2.1%
Systematic Uncertainty of A_{PV}	1.2%
Statistical Uncertainty of A_T	0.4 ppm
Detected Rate (each spectrometer)	140 MHz
CREX Production	35 days
Setup, Calibrations, Møller	10 days
Total Time Request	45 days

4 Beam Time Request

We request 45 days of polarized beam running in Hall A at 2.2 GeV using a new 4° degree septum magnets. This includes 5 days of commissioning and 5 days of overhead for Møller Polarimetry, transverse asymmetry, and auxiliary measurements. See Table 6. All beam for CREX production must be fully longitudinally polarized. We will need 2 days of beam vertically polarized for the transverse measurement and systematic checks.

References

[1] http://www.jlab.org/conferences/crex/

[2] C. Forssén, G. Hagen, M. Hjorth-Jensen, W. Nazarewicz, and J. Rotureau, Phys. Scr. T **152**, 014022 (2013).

[3] M. Bender, P.-H. Heenen, and P.-G. Reinhard, Phys. Rev. Mod **75**, 121 (2003).

[4] *Nuclear Physics: Exploring the Heart of Matter* (The National Academies Press, Washington, D.C., 2012).

[5] S. Bogner *et al.*, Comput. Phys. Comm. (2013); arXiv:1304.3713.

[6] P. G. Reinhard, W. Nazarewicz, Phys. Rev. C **81**, 051303 (2010).

[7] H.-W. Hammer, A. Nogga, A. Schwenk, Rev. of Mod. Phys. **85**, 197 (2013).

[8] S. Pieper, Phys. Rev. Lett. **90**, 252501 (2003).

[9] A.T.Gallant *et al.*, Phys. Rev. Lett. **109**, 032506 (2012)

[10] B. Frois et al., Phys. Rev. Lett. **38**, 152 (1977).

[11] C. Garcia-Recio, J. Nieves and E. Oset, Nucl. Phys. A **547**, 473 (1992).

[12] L. Ray, W. R. Coker, G. W. Hoffmann, Phys. Rev. C **18**, 2641 (1978).

[13] V. E. Starodubsky, N. M. Hintz, Phys. Rev. C **49**, 2118 (1994).

[14] B. C. Clark, L. J. Kerr, S. Hama, Phys. Rev. C **67**, 054605 (2003).

[15] A. Trzcinska et al., Phys. Rev. Lett. **87** , 082501 (2001).

[16] H. Lenske, Hyperfine Interact. **194**, 277 (2009).

[17] A.M. Bernstein, W.A. Seidler, Phys. Lett. B **34**, 569 (1971) Physics Letters B, **34**, Issue 7, 1971, Pages 569-571

[18] A.M. Bernstein, W.A. Seidler, Phys. Lett. B **39**, 583 (1972).

[19] T. W. Donnelly, J. Dubach, Ingo Sick, Nucl. Phys. **A503**, 589 (1989).

[20] C. J. Horowitz, Phys. Rev. C **57** , 3430 (1998).

[21] C. J. Horowitz, S. J. Pollock, P. A. Souder, R. Michaels, Phys. Rev. C **63**, 025501 (2001).

[22] B. G. Todd-Rutel and J. Piekarewicz Phys. Rev. Lett. 95, 122501 (2005).

[23] P.-G. Reinhard *et al.* in preparation.

[24] B. A. Brown, Phys Rev. Lett. **85**, 5296 (2000).

[25] C. J. Horowitz, J. Piekarewicz, Phys. Rev. **C64**, 062802 (2001).

[26] S. Gandolfi, J. Carlson, and Sanjay Reddy, Phys. Rev. C **85** 032801 (2012).

[27] F. Ozel, G. Baym, T. Guver, Phys. Rev. D **82**, 101301 (2010).

[28] A. W. Steiner, J. M. Lattimer, E. F. Brown, Astrophys. J. **722**, 33 (2010).

[29] C.J. Horowitz, J. Piekarewicz, Phys. Rev. **C66**, 055803 (2002).

[30] C. J. Horowitz, J. Piekarewicz, Phys. Rev. Lett. **86**, 5647 (2001).

[31] W. G. Lynch, M. B. Tsang, Y. Zhang, P. Danielewicz, M. Famiano, Z. Li, A. W. Steiner ArXiv:0901.0412.

[32] M.B.Tsang, Yingxun Zhang, P.Danielewicz, M.Famiano, Zhuxia Li, W.G.Lynch, A.W.Steiner, Phys. Rev. Lett. **102**, 122701 (2009).

[33] S. Abrahamyan *et al.*, Phys. Rev. Lett. 108, 112502 (2012).

[34] C.J. Horowitz, *et al.*, Phys. Rev. C 032501 (2012).

[35] M. Kortelainen, *et al.* Phys Rev. C**77** 064307 (2008).

[36] M. Kortelainen, *et al.* Phys Rev. C**82** 024313 (2010).

[37] J. Piekarewicz *et al.*, Phys. Rev. C **85**, 041302 (2012)

[38] J.Erler, N.Birge, M.Kortelainen, W.Nazarewicz, E.Olsen, A.M.Perhac, and M.Stoitsov, Nature **486**, 509 (2012).

[39] Y. Gao, J. Dobaczewski, M. ortelainen, J. Toivanen, and D.Tarpanov, Phys. Rev. C **87**, 034324 (2013).

[40] G. Hagen, *et al.*, Phys. Rev. Lett **109** 032502 (2012).

[41] G. Hagen, *et al.*, C-REX Workshop 2013, manuscript in preparation.

[42] A. Ekström, G. Baardsen, C. Forssén, G. Hagen, M. Hjorth-Jensen, G. R. Jansen, R. Machleidt, W. Nazarewicz, T. Papenbrock, J. Sarich, and S. M. Wild, Phys. Rev. Lett. (2003), in press; arXiv:1303.4674.

[43] J.D. Holt, *et al*, J. Phys. G **39** 085111 (2012).

[44] K. Hebeler and R.J. Furnstahl, Phys. Rev. C**87** 031302 (2013).

[45] I. Tews, T. Krueger, K. Hebeler, and A. Schwenk, Phys. Rev. Lett. **110**, 032504 (2013).

[46] S. N. More, *et al.* arXiv:1302.3815.

[47] H. De Vries *et al.*, Atomic and Nuc. Data Tables, **36** (1987) 495.

[48] I. Angelia and K.P. Marinova, Atomic and Nuc. Data Tables, **99** (2013) 69.

[49] A. Tamii et al., Phys. Rev. Lett. **107**, 062502 (2011).

[50] J. Birkhan *et al.* Dipole polarizability of ^{48}Ca from high resolution proton scattering at extreme forward angles RCNP experiment under analysis

[51] M. Gorchtein, C.J. Horowitz, Phys. Rev. C **77**, 044606 (2008).

[52] S. Abrahamyan, *et. al*, Phys. Rev. lett. **109**, 192501 (2012).

[53] C.F. Perdrisat, V. Punjabi, M. Vanderhaeghen, Prog. Part. Nucl. Phys. **59**, 694 (2007).

[54] A.V. Afanasev, S.J. Brodsky, C.E. Carlson, Y.-C. Chen, M. Vanderhaeghen, Phys. Rev. D **72**, 013008 (2005).

[55] K. A. Aniol *et al.*, Phys. Rev. Lett. **82** 1096 (1999). K. A. Aniol, *et al.*, Phys. Rev. C 69, 065501 (2004). K. A. Aniol, *et al.*, Phys. Rev. Lett. **96** 022003 (2006). A. Acha, *et al.*, Phys. Rev. Lett. **98** 032301 (2007).

[56] C.J. Horowitz, Phys. Rev. C **57**, 3430 (1998).

[57] L.W. Mo and Y.S. Tsai, Rev. Mod. Phys. **41**, 205235 (1969).

[58] M. Hauger *et al*, Nucl. Instr. and Methods A 462 (2001) 382.

[59] M. Friend *et al.*, Nucl. Instr. and Methods A 676 (2012) 96.

[60] J.E. Wise *et al.*, Phys. Rev. **C 31**, 1699 (1985).

[61] Jefferson Lab Experiment E12-11-101 (PREX-II). Proposal available at http://hallaweb.jlab.org/parity/prex

[62] P. G. Reinhard *et al.*, Private Communication.